CrystEngComm

HIGHLIGHT

View Article Online
View Journal | View Issue

Cite this: *CrystEngComm*, 2025, **27**, 6719

Liquid–liquid phase separation into reactant-rich precursors during mineral crystallization

David Carriere,* Jade Raimbault, Mark A. Levenstein and Corinne Chevallard

Liquid–liquid phase separation (LLPS) is being increasingly recognized as a critical intermediate step in non-classical crystallization pathways, representing a paradigm shift from early descriptions invoking single-step nucleation. While extensively documented in organic compounds, LLPS in mineral systems presents unique experimental challenges due to accelerated crystallization kinetics, thus complicating physical characterizations (viscosity, chemical composition, *etc.*). This review synthesizes current evidence for LLPS across diverse mineral systems, examining cases by decreasing order of experimental confidence—from the well-known calcium carbonate system to emerging discussions in oxalates, oxides, metallic nanoparticles, sulfur sols, sulfates, calcium phosphates, metal organic frameworks and sodium chloride. A fundamental challenge lies in definitively establishing liquid character, as cryogenic Transmission Electron Microscopy (TEM) and X-ray scattering methods cannot distinguish between liquid and solid amorphous structures, while liquid-phase TEM observations are prone to interfere with the real crystallization process. Understanding when and why LLPS occurs remains challenging, complicated by inconsistent reporting practices and the predominant use of thermodynamic interpretations where kinetic factors may actually govern the process. Operating far from equilibrium, these systems may require alternative mechanisms beyond classical thermodynamic treatments. Key research frontiers include rigorous demonstration of true liquid character, systematic exploration of structure and dynamics across mineral systems down to the atom and sub-millisecond scales, and integrated experimental–theoretical approaches capturing both thermodynamic and kinetic factors—essential for the rational design of materials and controlled nanoparticle morphologies through LLPS-mediated pathways.

Received 11th July 2025,
Accepted 18th September 2025

DOI: 10.1039/d5ce00695c

rsc.li/crystengcomm

1. Introduction

The crystallization of solutes represents a fundamental process ubiquitous across natural and industrial systems. Contemporary understanding establishes that crystallization proceeds predominantly through multistep pathways rather than 'classical', single-step mechanisms. As Vekilov aptly noted in 2020,[1] "two-step nucleation is by now ubiquitous and registered cases of classical nucleation are celebrated", highlighting the paradigm shift in crystallization theory over recent decades. This evolution in understanding has been comprehensively documented in several landmark reviews that have shaped the field's trajectory, including foundational works among others by Gebauer and Cölfen (2011)[2] and De Yoreo *et al.* (2015).[3]

Among the transient states identified in non-classical crystallization pathways (solid-state amorphous particles, clusters, nanocrystals, *etc.*), dense reactant-rich liquid precursors formed *via* liquid–liquid phase separation (LLPS) have been particularly discussed. LLPS holds special interest for the crystallization community as it potentially enables the rational design of synthetic crystalline (nano)materials and the understanding of natural phenomena (biomineralization, geological processes), while simultaneously challenging established theoretical frameworks.

While LLPS has been extensively reviewed and documented in organic systems, particularly proteins and molecular assemblies,[4,5] where droplets formed by LLPS can develop to macroscopic dimensions, the phenomenon in inorganic or mineral systems has received comparatively less systematic attention. The calcium carbonate system represents the seminal example of mineral LLPS, establishing the foundational framework for understanding liquid–liquid phase separation in inorganic crystallization.[6] Beyond this well-documented case, various mineral systems—some discovered even prior to $CaCO_3$—have been reported to exhibit LLPS behavior, expanding the scope of non-classical crystallization pathways across diverse inorganic compositions.

Université Paris-Saclay, CEA, CNRS, NIMBE, LIONS, 91191 Gif-sur-Yvette, France. E-mail: david.carriere@cea.fr

However, direct observation and characterization of LLPS in mineral systems presents significantly greater experimental challenges than compared to those of their organic counterparts. These challenges arise primarily from accelerated crystallization kinetics that drastically limit the temporal window for detection and analysis, often reducing observable lifetimes to milliseconds or seconds rather than the minutes or hours typical in organic systems. Additionally, distinguishing between amorphous solid precursors and true liquid droplets based on dynamic information remains technically demanding, requiring sophisticated experimental approaches compatible with the short lifetime of these transient states. As a consequence, the experimental conditions and mechanisms governing mineral LLPS remain debated, creating a significant knowledge gap in our understanding of non-classical crystallization pathways.

This review aims to address these knowledge gaps by synthesizing existing evidence and identifying common patterns in LLPS behavior across various mineral systems, while critically evaluating the degree of confidence with which LLPS has been demonstrated in different minerals. We describe the systems by decreasing degree of confidence—as we perceive and justify it—examining the proposed mechanisms of LLPS, the transition to more stable mineral phases, and highlighting promising research perspectives for future investigation (Fig. 1).

2. Reported mineral systems exhibiting LLPS

The following sections critically examine the current inventory of mineral systems where LLPS has been reported, with particular attention to the experimental basis, reproducibility, and reliability of each claim. We summarize our literature analysis in Table 1 and justify the degree of confidence in the occurrence of LLPS in the corresponding sections.

2.1. Calcium carbonate and other carbonates

Reports of mineral liquid–liquid phase separation prior to crystallization are by far dominated by studies on $CaCO_3$, where LLPS has been postulated then confirmed experimentally or numerically. For the sake of clarity, we discuss here some reports on "pre-nucleation clusters" (PNCs, see below), even if the author(s) have not discussed liquid–liquid phase separation.

Either PNCs or LLPS have been reported for crystallization from all the common preparation methods, either in the presence or absence of polymer additives: 1) *in situ* production of CO_2 in a $CaCl_2$ aqueous solution, by reaction of dimethyl carbonate with NaOH,[46] 2) the Kitano method, where a saturated solution of calcium bicarbonate precipitates $CaCO_3$ upon slow evaporation of water or

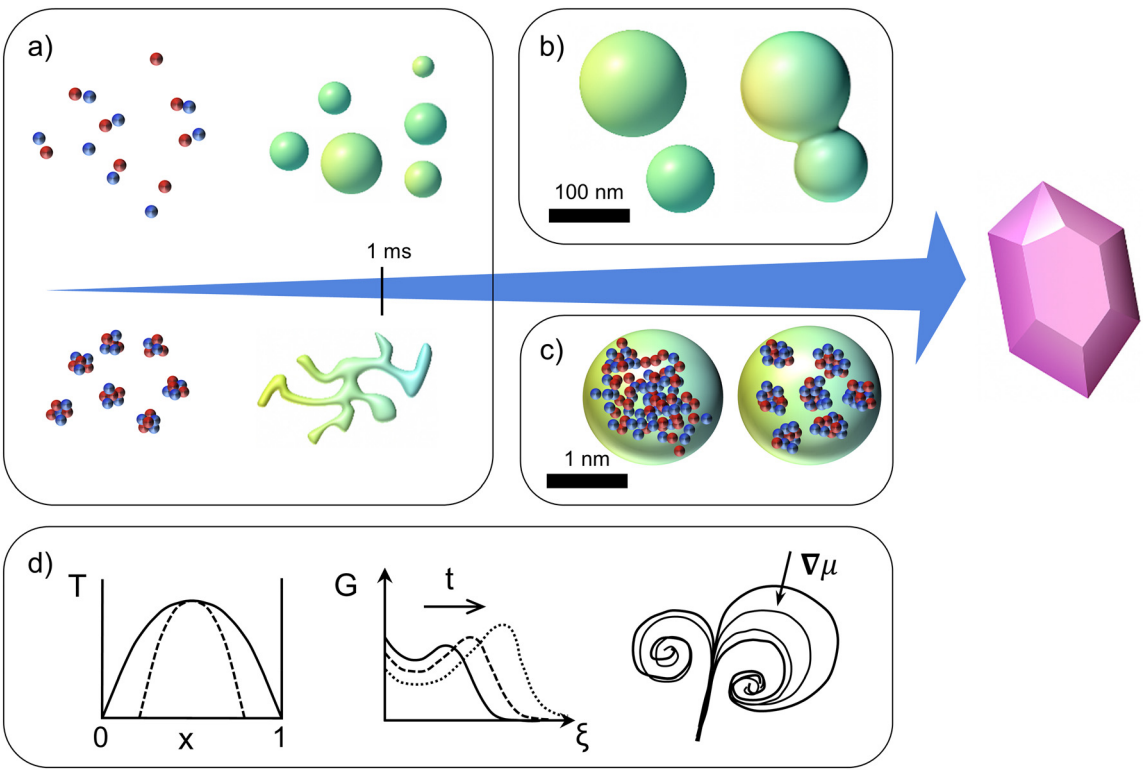

Fig. 1 Key challenges in the field of liquid–liquid phase separation prior to crystallization: a) capturing with atomic to nanometer scale and sub-millisecond resolution the concentration fluctuations in the unstable parent solution and the forming structures; b) measuring the viscosity of the liquid phase; c) characterizing the atomic-scale structure of the liquid; and d) identifying or developing a suitable theoretical framework.

Table 1 Summary of mineral systems with reported LLPS, the techniques used to provide evidence, and our confidence assessment for each demonstration. Only selected references are shown for clarity. See text for complete analysis

System	Supporting techniques	Confidence for LLPS
Calcium carbonate (no additives)	Liquid-like morphology[7–10] (SEM, cryo-TEM), diffusion dynamics[11,12] (NMR, MD) Growth dynamics[13] (SEM) Droplet coalescence[14] (LP TEM)	Very high. Debate on condensation of ion pairs *vs.* pre-nucleation clusters
Calcium carbonate (with additives)	Liquid-like morphology in bulk, on surfaces and in porous matrices[6,15–21] (SEM, cryo-TEM, AFM) Diffusion dynamics (NMR[11]) Droplet coalescence (LP TEM[22])	Very high. Polymer-stabilized colloidal liquid
Cerium oxalate	Liquid-like morphologies in bulk and porous matrices (SEM, cryo-TEM),[23–25] droplet coalescence[25] (LP TEM)	Very high
Metal nanoparticles	Liquid-like morphologies in bulk and on surfaces[26,27] (cryo-TEM), soft droplets deposited on substrates[27] (AFM), liquid-like dynamics[28–30] (LP TEM)	Very high. Possible colloidal liquid
Apatite	Liquid-like morphology in bulk, and in porous matrices[31–33] (SEM, cryo-TEM), dense liquid (LP TEM)[34,35]	Supportive. Granular structure not systematically assigned to colloidal liquid
Barium sulfate	Liquid-like morphologies[36,37] (TEM)	Suggestive, static images after ethanol quenching and drying under vacuum
Sulfur hydrosols	Macroscopic behavior of an emulsion[38,39]	Suggestive (thermal behavior), lack of sub-micrometer dynamical characterizations
Oxides	Liquid-like morphologies in bulk[40,41] (cryo-TEM)	Tentatively supportive. Colloidal liquid postulated
Metal organic frameworks	Amorphous phase (electron and X-ray diffraction),[42–45] morphology (cryo-TEM)[45]	Tentatively supportive

decrease in CO_2 partial pressure,[7,8,47,48] 3) the ammonia diffusion technique, where thermal decomposition of ammonium carbonate initiates diffusion of carbon dioxide and ammonia into an aqueous $CaCl_2$ solution,[6,15,17,20,21,49–55] and 4) direct mixing,[9–11,13,14,18,19,22,56–62] where an aqueous solution of calcium chloride is mixed with a (bi)carbonate solution. This final method allows controlling the precursor concentrations, the initial pH of the (bi)carbonate solution, the pH during the whole mineralization process (by titration and simultaneous addition of NaOH/HCl), injection speed, and is easily implemented with various characterization techniques.

Similarly, for simulations,[10,12,22,47,57,63–65] it is essential to keep track of the conditions under which the various results were obtained—not only the total simulation time (often on the order of tens of nanoseconds), but also the strategies used to explore the configurational landscape within available computational time. Two strategies include 1) initializing the system at artificially high ion concentrations to enhance

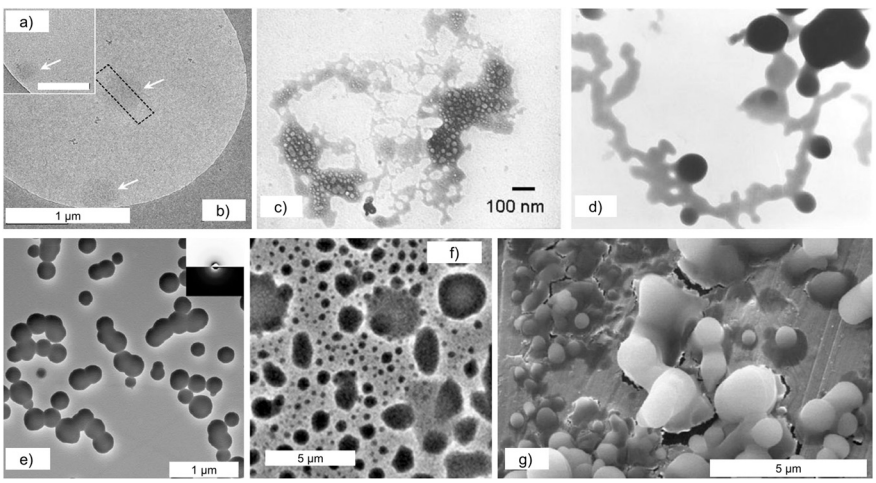

Fig. 2 Experimental investigation of LLPS in $CaCO_3$. a and b) Cryo-TEM of a carbonate buffer solution titrated with a $CaCl_2$ solution. Adapted with permission from Smeets *et al.*[10] Copyright 2017 National Academy of Sciences. c and d) Cryo-TEM of carbonate and $CaCl_2$ solutions mixed rapidly, frozen after 100 ms and 2 min after reaction, respectively. Adapted from Rieger *et al.*[9] with permission from The Royal Society of Chemistry. e) TEM of a calcium carbonate solution collected 400 s into the evaporation process (Kitano method). Adapted with permission from Wolf *et al.*[8] Copyright 2011 American Chemical Society. f) LP TEM of carbonate and $CaCl_2$ solutions *ca.* 500 s after mixing in the observation cell. Adapted with permission from Ramnarain *et al.*[14] Copyright 2022 American Chemical Society. g) SEM of carbonate and $CaCl_2$ solutions mixed gently, 1 min after mixing. Adapted from Rieger *et al.*[9] with permission from The Royal Society of Chemistry.

sampling efficiency, then transferring to lower concentrations or reconstructing free energy profiles to account for finite-size and concentration effects[57,65] and 2) simulating directly dilute conditions with enhanced sampling techniques[10,12,63] and/or computationally less demanding methods.[47,64]

For clarity of presentation, we begin by analyzing reports of LLPS occurring in the absence of organic additives, before turning to the reports in presence of additives, including the so-called PILP (polymer-induced liquid precursor), although PILPs were historically first described.

2.1.1. LLPS in $CaCO_3$ without additives.

Evidence for the liquid state. Dense liquid precursor formation was initially inferred from solid morphologies exhibiting "liquid-like" characteristics after reaction (Fig. 2). SEM analysis revealed solid deposits on substrates exhibiting morphologies suggestive of liquid droplets that were arrested during coalescence (Fig. 2g). At shorter reaction times, transmission electron microscopy after regular grid preparation (TEM) or under cryogenic conditions (cryo-TEM) provided images of reactive mixtures prior to crystallization that consistently show "liquid-like" or "emulsion-like" structures, strongly suggesting liquid-phase intermediates before solidification (Fig. 2a–e).[7–10] Supporting this interpretation, Zou *et al.* demonstrated that amorphous calcium carbonate (ACC) particle size distributions align with spinodal decomposition predictions,[13] indicating liquid–liquid phase separation followed by isomorphic transition to solid ACC. In several papers, Wolf emphasized the role of electrostatically stabilized liquid droplets to explain the lack of coalescence up to macroscopic sizes.[7,8,66]

To unambiguously assess the liquid character of transient structures, viscosity measurements represent the most direct approach. Bewernitz *et al.* reported two diffusion coefficients measured by nuclear magnetic resonance (NMR) in calcium chloride/NaOH-titrated carbonate solutions, assigning the slower coefficient (5×10^{-6} cm^2 s^{-1}) to liquid structures—only a factor of 2 lower than coexisting (bi)carbonate species in water.[11] Molecular dynamics simulations provide detailed insights into liquid properties: computed ion diffusivity ranges from 10^{-7} to 10^{-8} cm^2 s^{-1}, representing two orders of magnitude higher mobility than in amorphous $CaCO_3{\cdot}H_2O$, yet two to three orders of magnitude lower than ions in solution.[10,12,22]

More recently, Ramnarain *et al.* (2022) directly visualized coalescence of these structures using liquid-phase TEM (LP TEM), providing the first unequivocal evidence of their liquid nature (Fig. 2f).[14] While the existence of liquid structures is now well-established, direct experimental characterization of their rheological properties remains limited. Nevertheless, the available evidence—spanning diffusion measurements, molecular dynamics predictions, and direct visualization—conclusively validates the initial hypothesis of liquid precursors originally based on indirect morphological observations.

Chemical composition of the dense liquid phase. Molecular dynamics simulations give insight on the composition of the dense liquid phase: calcium ions are coordinated by 4–7 H_2O molecules—fewer in the core and more at the periphery of the droplet—bound to 2–3 carbonate ions, and an increase in coordination number correlates with an increase in the viscosity of the liquid.[10,12] The speciation of (bi)carbonate in the dense liquid phase has attracted much interest, with early reports concluding that the liquid is enriched in bicarbonate relative to its concentration in the parent solution.[11] More detailed studies on the (bi)carbonate composition in the dense liquid phase are available, but in the presence of additives (see below).

2.1.2. Prenucleation clusters *vs.* ion pairing: the problem of calcium activity reduction. There is a broad consensus that before reaching the binodal for LLPS, the activity of free Ca^{2+} ions measured by ion-selective electrode potentiometry is significantly reduced compared to the ideal solution, and varies linearly with added Ca^{2+} concentration until nucleation starts.[10,11,56,57] The observed reduction in activity has been attributed to 30% to more than 60% of Ca^{2+} ions being sequestered in complexes. This experimental result has sparked intense debate regarding its origin, and questions whether a classical thermodynamic description of liquid–liquid phase separation is correct, or if clusters with specific thermodynamic properties need to be invoked.

The two competing interpretations to explain the reduction in calcium activity are:

1) sequestration in calcium (bi)carbonate ion pairs. This was reported as compatible with both regular solution theory and classical nucleation theory,[10,47] the latter expecting that the concentration of ion pairs exceeds that of larger aggregates by orders of magnitude.

2) sequestration in pre-nucleation clusters (PNCs).[11,48,56–60,65,67] Their specific properties have been refined over time, to reach the current status:[67] PNCs are defined as disordered nanometer-sized oligomers of several tens of calcium (bi)carbonate moieties; they are reported to form in both under- and supersaturated solutions with respect to the first nucleating species (amorphous calcium carbonate); at fixed supersaturation, their size distribution remains time-independent; as supersaturation increases, the distribution shifts to larger sizes, and the dynamics (mobility inside the PNCs and rate of exchange with coexisting ion pairs) slows down.

The debate between both interpretations is still lively as illustrated by two recent reports on the matter.[10,67] In the initial report of Gebauer *et al.*[56] and subsequent work,[11,48] oligomerization has been supported by analytical ultracentrifugation (AUC), with sedimentation coefficients compatible with monodisperse 2 nm-sized clusters (≃70 calcium atoms). Authors have, however, acknowledged that the sedimentation was only detected above saturation with respect to the nucleating phase, and that "the clusters cannot be detected in the undersaturated stage of the experiments", despite the reduction in activity already being evident in this stage. Overlooking the metrological details of size determination, one can also reasonably object, like Smeets

et al.,[10] that nucleation could happen during centrifugation (>8 h in Gebauer *et al.*,[56] unreported in Bewernitz *et al.*[11]). To our knowledge, evidence for or against nucleation 8 h after arrested titration has not been discussed in depth – presumably, owing to the difficulty in mitigating CO_2 degassing and maintaining constant supersaturation over such extended periods of time.

Later work has reported direct observation of PNCs by cryo-TEM, showing 0.6 nm sized structures trapped in vitreous ice.[48] However, a subsequent analysis of the operation conditions has shown that the achieved resolution was significantly above 1 nm.[10] An attempt to observe PNCs with better resolution failed, which is compatible with either the ion pair interpretation, or the loss of PNCs upon grid preparation. In any case, if PNCs exist for $CaCO_3$, their size is significantly smaller than the 2 nm estimated by AUC.

Support to either confirm or disprove PNC formation has been actively pursued through computational approaches. On one hand, Demichelis *et al.* reported PNCs in molecular dynamics with calcium concentrations in the 60 mM to 500 mM range during 50 to 70 ns, which could be observed within 1 ns after transfer to a 0.4 mM concentration.[65] They, however, also reported that the PNCs do not form spontaneously in the 1 ns time window when simulated at 0.4 mM. On the other hand, Smeets *et al.*[10] demonstrated that all initial configurations (random ion distributions and clusters) relax towards ion pairs in the 20–40 mM concentration range and 20–60 ns simulation time, with no significant clustering. Prominent ion pairing was later confirmed by Monte Carlo simulations using mean force potentials and validated experimentally by X-ray absorption spectroscopy.[47] However, Gebauer has highlighted a fundamental challenge in bridging density functional theory calculations to molecular mechanics approaches, questioning the seamless integration of different computational scales and their collective ability to accurately represent PNCs behavior in solution.[67]

Additionally, PNCs formation has been rationalized with a chemical equilibrium model where clusters are produced by attachment /detachment of calcium carbonate ion pairs, each of the equilibria having an identical chemical constant independent of the cluster size,[56] compatible with both measured enthalpies and activity reduction.[11,56] However, this model alone is not discriminant as it remains compatible with all clustering sizes – including simple ion pairing. On the contrary, Smeets *et al.* have calculated that standard thermodynamic databases of calcium carbonate are sufficient to account for the reduced calcium activity without invoking clustering other than ion pairing, provided the ion–ion electrostatic interactions are correctly taken into account in the speciation model. They therefore produced a state-of-the-art speciation calculation without invoking additional thermodynamic species like PNCs. It is however not perfectly clear if this rules out the existence of PNCs, as part of the thermodynamic constants used have been constructed by fitting solubility values to experimental data, assuming there are no PNCs.

In summary, the debate surrounding pre-nucleation clusters (PNCs) remains active and will likely require continued experimental developments at synchrotron sources, reassessment of thermodynamic databases, and new theoretical considerations to be fully resolved. Notably, the term "pre-nucleation cluster" has gained widespread acceptance regardless of the preferred mechanistic hypothesis, reflecting the consensus that calcium activity is indeed reduced in these systems. The fundamental disagreement centers not on the sequestration of ions into larger assemblies (potentially reduced to ion pairs), but rather on their thermodynamic interpretation: whether PNCs represent entities with special thermodynamic status distinct from classical theory, or whether they simply describe the sub-critical clusters already encompassed by both classical nucleation theory and regular solution theory.

2.1.3. Thermodynamic description of LLPS. While consensus exists regarding the overall consistency of LLPS observations with thermodynamic equilibrium phase diagrams—even when PNCs have been reported—specific mechanistic details remain actively debated. Evidence for spinodal decomposition has been inferred from characteristic TEM morphologies[9] and from the systematic variation of ACC particle sizes with supersaturation levels.[13] Conversely, nucleation-based mechanisms are supported by size evolution studies as a function of temperature[46]—albeit in polymer-modified systems—and have been proposed as a reasonable assumption whenever supersaturation increases slowly.[10]

The critical temperature of the phase separation remains debated, with conflicting evidence supporting both low and high temperature scenarios. A low critical temperature has been proposed based on ACC size evolution with temperature in polymer-containing systems[46] and ACC solubility–temperature relationships.[59] In contrast, a high-temperature critical point appears more compatible with size variations observed under different supersaturation conditions[13] and has been postulated from the retrograde solubility behavior of calcium carbonate.[12]

2.1.4. LLPS in $CaCO_3$ with additives. The investigation of liquid–liquid phase separation in calcium carbonate systems has been extensively documented in the presence of polymers (Fig. 3).[7–9,11,14,15,17,18,20,21,46,49–55,58,62,68] Liquid precursors in polymer-supplemented systems were first reported by L. Gower in $CaCO_3$ biomineralization studies.[6,15] Using gas diffusion methods, 20 mM $CaCl_2$ solutions containing 20 ppm sodium polyaspartate (MW = 8600 Da) were exposed to $(NH_4)_2CO_3$ vapors. Gower observed dense liquid droplets at the solution–air interface, visible to the naked eye. While lacking published video evidence,[69] her seminal work provided indirect proof of liquid behavior:[15] droplets coalesced on glass substrates, where inspection by Scanning Electron Microscopy (SEM) revealed homogeneous micron-thick films with some solidified droplets remaining unmerged (Fig. 3c). These initially amorphous films subsequently crystallized into large (10–100 μm) iso-oriented or spherulitic domains. The initially amorphous film exhibits

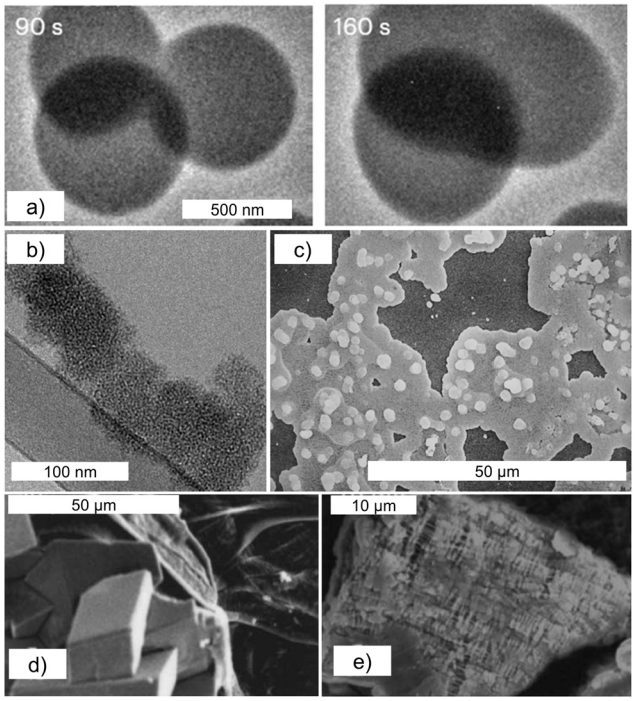

Fig. 3 Experimental investigation of LLPS in $CaCO_3$ in presence of polymers. a) LP TEM of a coalescence event. Adapted with permission from Jin *et al.*[22] Copyright 2024 Springer Nature. b) Cryo-TEM of a solution aliquot after 200–250 min infusion. Adapted with permission from Xu *et al.*[21] Copyright 2018 Springer Nature. c) SEM image of a glass substrate in contact with $CaCl_2$ + polyaspartate solution exposed to ammonium carbonate vapor (ammonia diffusion method, reaction time not recorded). Adapted from Gower *et al.*,[15] with permission from Elsevier. d) Collagen I matrix exposed to a calcium carbonate solution, without polymer, unrecorded reaction time (>3 days) and e) with poly(acrylic acid), after 15 days. Adapted with permission from Olzsta *et al.*[16] Copyright 2003 Springer.

space-filling nanoparticles (30–100 nm) that crystallize pseudomorphically, preserving film compactness and nanogranularity. This nanostructuring resembles biominerals,[70] enabling diverse morphologies for biological function while indirectly supporting liquid precursor behavior. Additionally, after testing the infiltration capacity of the dense liquid precursor, they reported that porous matrices are completely mineralized when $CaCO_3$ forms in the presence of polyaspartic acid, whereas in the absence of polymer, micron-sized $CaCO_3$ crystals only deposit at the surface without invading the scaffold (Fig. 3d and e).[16] This was taken as an additional proof for liquid phases to form.

Polymer addition suppresses direct crystal nucleation, enabling non-crystalline morphologies to develop through highly hydrated intermediates. This polyelectrolyte-induced liquid transient was termed PILP (polymer-induced liquid precursor).[15] Various research teams have since reported liquid transients during $CaCO_3$ synthesis using diverse additives: sodium polyacrylate,[17,21,55] polycarboxylates,[9] double-stranded DNA,[21,54] ovalbumin,[8,49,53] oligopeptides,[52,63] poly(allylamine hydrochloride).[21,51] The latter involves a positively charged polyelectrolyte, contrasting with other studies using negatively charged polyelectrolytes that mimic carboxylate-rich biopolymers in biomineralization.

Owing to the difficulty of directly observing transient liquid structures during syntheses, their liquid nature has most often been inferred from characteristic non-crystallographic morphologies (such as films, helices, and cylindrical nanorods),[6,15] their ability to infiltrate nanometric pores,[16,18] or their selective wetting behavior on various substrates.[17,20,55] Berg *et al.* notably characterized PILP phase wetting on electrospun fibers functionalized with different chemical groups:[55] OH-functionalized fibers exhibited full wetting (zero contact angle), while amine-functionalized surfaces induced non-wetting behavior (contact angle >150°). As with additive-free $CaCO_3$ systems, direct confirmation of liquid character emerged only recently, with coalescence events confirmed by Jin *et al.* in 2024 by LP TEM (Fig. 3a).[22]

The dense liquid phase was initially interpreted as a coacervate from polymer phase micro-separation with counter-ion calcium (for negatively charged polymers)[52,70] or carbonate (for positively charged polymers).[51] This was considered a direct consequence of polyelectrolyte addition. However, NMR detection of intermediate liquid phases both with and without polymer additives challenged this view.[11] Current understanding shows that polymers primarily stabilize developing liquid phases against amorphous conversion rather than altering underlying thermodynamics or shifting binodal lines.[8,58,63] This supports Faatz *et al.*'s original hypothesis that LLPS can occur in $CaCO_3$ systems without polymers, despite their experiments using additives.[46]

Several studies have attempted to characterize the composition and viscoelastic properties of the liquid phase.[11,19,50] However, characterization remains limited due to time-dependent composition changes from progressive water and polymer ejection.[50] The bicarbonate–carbonate composition remains debated: Bewernitz *et al.* reported bicarbonate enrichment in dense liquid structures relative to reactant-poor solutions,[11] while Jin *et al.* recently detected only bicarbonate at high pH, with composition $Ca(HCO_3)_2{\cdot}nH_2O$ (n = 7.5 ± 1.7).[22] This contrasts with recent NMR reports indicating carbonate-rich phases.[61] Similar to cerium oxalate (see below), the viscosity estimated from coalescence events directly recorded by LP TEM is reported to be nine orders of magnitude larger than water.[22]

Recent observations have questioned the "true" liquid nature of the PILP phase: the absence of intermediate contact angles, gel-like elasticity in AFM measurements,[19] and nanogranularity in all PILP-formed structures (Fig. 3b).[21,68] Cryo-TEM and NMR studies by Sommerdijk and coworkers on various polymer additives revealed no liquid phase but the systematic presence of *ca.* 50 nm amorphous clusters composed of 2 nm nanoparticles. They concluded that "PILP is actually a polymer-driven assembly of ACC clusters, and [that] its liquid-like behavior at the macroscopic level is due to the small size and surface properties of the assemblies". The authors suggested redefining PILP as "polymer-induced

liquid-like precursor". Similarly, Gower coined the process "colloid assembly and transformation (CAT)" in 2017.[68] Recent LP TEM studies with non-polymer additives confirm structural differences between polymer-free and polymer-stabilized LLPS:[14,21] the former generates truly homogeneous liquid droplets of ion complexes, while the latter produces polymer-stabilized nanoparticle assemblies that change dynamically in shape.

In summary, like for additive-free calcium carbonate crystallization, LLPS propositions based on indirect observations have been validated by recent LP TEM characterization. However, the process involves colloidal assembly rather than a dense molecular liquid, though the nature of this shift in the presence of polymer remains unclear and certainly calls for active research.

2.1.5. Other metal carbonates. PILP has been observed in Sr and Ba carbonates in the presence of poly(acrylic acid). The liquid character was assessed through the morphology of films on substrates by polarized light microscopy and the ability to spin fibers from solution.[71] Although insights obtained with similar techniques were ultimately proven correct for $CaCO_3$ PILP, the evidence for a liquid state remains indirect for these metal carbonates. However, this similarity was further confirmed when Wolf *et al.* claimed LLPS in Sr, Ba, Mn, Cd, and Pb carbonates. These findings are based on conventional TEM observations of specimens prepared from droplets of saturated solutions (supernatants) that were gradually concentrated through acoustic levitation. The liquid character has been assigned based on the liquid-like morphologies and because 'the low contrast variation inside of the particles indicates their liquid-like state'.[66] Concluding on the liquid state appears reasonable given the consistency with the abundant $CaCO_3$ literature and the reported PILP behavior of Ba and Sr phases. However, studies on metal carbonate systems remain scarce and would benefit significantly from direct liquid-phase TEM investigations or at least cryo-TEM observations, especially since some of the shapes in the initial report deviate significantly from typical smooth structures expected for droplets, even under shear.

2.2. Cerium oxalate

In calcium oxalate systems, the stabilization of amorphous forms is well-established and undebated.[72] However, the existence of a liquid state remains undemonstrated. While hints for LLPS have been reported, the authors acknowledged the uncertainty of these observations and called for further investigation.[73] More compelling evidence has emerged from cerium oxalate studies, where LLPS was initially inferred from the characteristic morphologies observed in filter deposits (Fig. 4a and b).[23] Subsequent cryo-TEM revealed distinctive beaded morphologies consistent with liquid precursor formation (Fig. 4c).[24,74] The liquid nature of these phases was definitively established through direct liquid-phase TEM observations: analysis of coalescence events between liquid precursor droplets led to the determination of a viscosity of approximately 100 Pa s—several orders of magnitude higher than that of water (Fig. 4d).[25] This quantitative viscosity provided definitive proof of the liquid state of the transient species, while highlighting that liquid-like behavior at the nanoscale may appear highly viscous macroscopically. Although composition assessment remains lacking, this system shows great promise for fundamental advances in non-classical crystallization.

2.3. Metal nanoparticles

In the laboratory, metal nanoparticles are predominantly synthesized by reduction of a metal salt solution by another

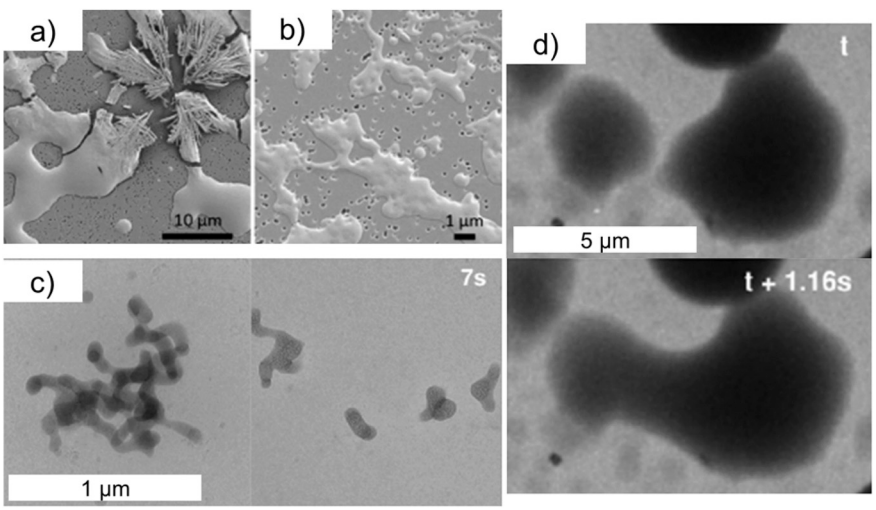

Fig. 4 Experimental investigation of LLPS in cerium oxalate. a and b) SEM of deposits collected on top of a 0.2 µm pore filter membrane. Repoduced from Rodríguez-Ruiz *et al.*[23] with permission from The Royal Society of Chemistry. c) Cryo-TEM of a freeze-quenched solution 7 s after reaction. Adapted with permission from Raimbault *et al.*[25] Copyright 2024 American Chemical Society. Identical image sizes. d) LP TEM of a coalescence event between two droplets wetting the observation window. Adapted with permission from Raimbault *et al.*[25] copyright 2024 American Chemical Society. The two images are separated by *ca.* 1.2 s.

additive. In the case of gold, Mikhlin *et al.* reported in 2009 liquid–liquid phase separation during the reduction of tetrachloroaurate by citrate in water. Indirect evidence was first obtained based on structures with liquid-like morphology found by TEM of dried aliquots,[26] and direct evidence was soon obtained using Atomic Force Microscopy (AFM) in liquid phase (Fig. 5).[27] It is clear that gold forms *via* structures with sizes in the 100 nm range that deposit on the observed surface, reported as "liquid or soft matter since they are easily stretched by [the] moving cantilever". The composition of the liquid has been confirmed later to consist of Au_nCl_{n+x} clusters.[75]

Transmission electron microscopy cannot investigate additive-induced gold reduction syntheses because the electron beam dominates the reduction process. However, liquid-phase electron microscopy has become an extremely convenient *in situ* characterization tool using the beam as the electron source. Loh *et al.* reduced tetrachloroaurate by a TEM electron beam, and observed the formation of liquid structures of tens of-nanometers, rich in hydrated gold complexes with an estimated 4 M concentration (Fig. 5a).[28] Jin *et al.* later observed similar structures by liquid-phase TEM, and additionally reported nanocrystals embedded in the parent Au-rich liquid phase (Fig. 5b and c).[29]

Liquid–liquid phase separation has been reported for other metal nanoparticles including silver[28] and platinum.[30] In palladium (Fig. 5f–i), additional substructure was resolved within the liquid: the liquid phase was characterized as a "cluster cloud"—a disordered, dynamic assembly of nanometer-sized amorphous cluster (Fig. 5f and g).[29] For nickel nanoparticles, Yang *et al.* describe amorphous particles with "randomly packed granular features" resembling LLPS with cluster clouds, although they make no explicit LLPS connection.[76]

The generality of LLPS in metal ion solutions upon reduction both induced chemically and by liquid-phase TEM makes little doubt. However, challenges remain regarding the appropriate mechanistic description. Loh *et al.* notoriously proposed that the gold-rich liquid forms by spinodal decomposition. However, the lack of quantitative data prevented validation through, for example, the expected structure factors. As they acknowledged, confinement in LP TEM cells slows diffusion processes by orders of magnitude, potentially changing the rate-limiting step compared to bulk syntheses. Regarding the presence of the 'cluster cloud' outside a TEM, a positive indication was given by Ramamoorthy *et al.*[77] They used Small-Angle X-ray Scattering (SAXS) to evidence aggregates containing 15–70 Au atoms in organic gold precursors before reduction (tetrachloroaurate stabilized by oleylamine in hexane). They described these nanometer-scale structures as pre-nucleation clusters, referencing well-known $CaCO_3$ observations. Although they did not report possible aggregation into liquid phases, this may indicate a common driving force between PNCs at equilibrium prior to reaction and the amorphous primary

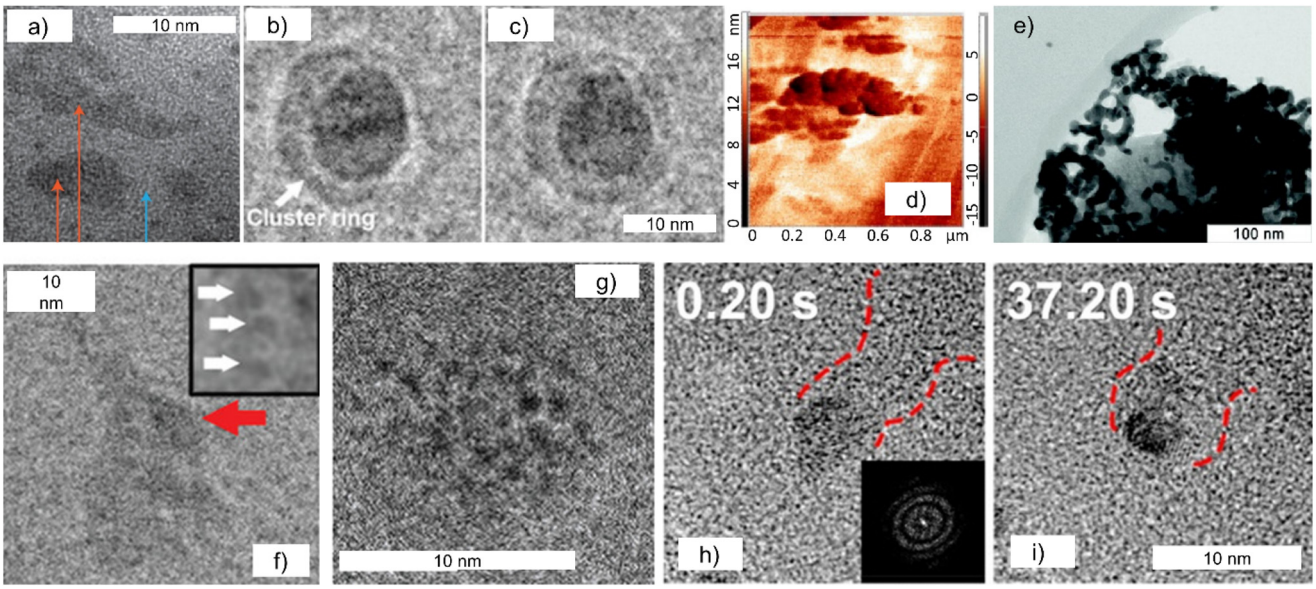

Fig. 5 Experimental investigation of LLPS in syntheses of metal nanoparticles. a) LP TEM of a $HAuCl_4$ aqueous solution. Blue arrow: gold-poor liquid. Orange arrows: gold-rich structures. Adapted with permission from Loh *et al.*[28] Copyright 2017 Springer Nature. b and c) LP TEM of a $HAuCl_4$ aqueous solution. The arrow indicates the structure assigned to a dense liquid corona made of nanometer-sized clusters. Adapted with permission from Jin *et al.*[29] Copyright 2019 Wiley-VCH. d) Liquid-cell AFM of mixture of aqueous $HAuCl_4$ and sodium tricitrate in contact with a graphite substrate, imaged 150 min after mixing. Adapted with permission from Mikhlin *et al.*[27] Copyright 2011 Elsevier. e) Same by TEM f and g) LP TEM of a Na_2PdCl_4 aqueous solution. The red arrow indicates a darker structure assigned to a crystal nucleus. The inset shows nanometer-scaled structures assigned to ultrasmall clusters constituting the liquidlike 'cloud'. Adapted with permission from Jin *et al.*[29] Copyright 2019 Wiley-VCH. h and i) LP TEM of a solution of palladium(II) 2,4-pentanedionate in methyl pyrrolidone. Red dashed lines outline the dense liquid structure around the nanocrystal. Adapted with permission from Li *et al.*[30] Copyright 2021 American Chemical Society.

units of the "cluster cloud", but more direct evidence with simultaneous validation by TEM would be beneficial.

2.4. Sodium chloride

Molecular dynamics simulations of NaCl crystallization have provided valuable insights into the morphological transitions associated with liquid–liquid phase separation.[78–80] In the metastable region between the binodal and spinodal curves, simulations reveal the formation of isolated rock salt clusters that fluctuate in a manner consistent with the 'classical', single-step classical nucleation theory. Jiang *et al.*,[78] Finney *et al.*[79] and Bulutoglu *et al.*[80] cautiously describe the emerging structures as "liquid/amorphous", "liquid-like" and "amorphous" respectively, without further discussing their viscosity. Of note, the clusters are dehydrated NaCl condensates – which suggests viscosity orders of magnitude above water – but nucleation has been predicted within 70 ns of simulation – which also suggests it still remains sufficiently low to allow crystallization. Further investigation is therefore needed to qualify their true liquid-like character. Above the spinodal threshold (*ca.* 18 mol kg^{-1}), the system further exhibits the expected interconnected non-crystalline clusters of NaCl condensates that form barrierless, in which the NaCl crystals nucleate with an activation barrier (Fig. 6). This consensus among simulations highlights the extreme challenge of experimentally capturing these events, which occur in well under one microsecond.

2.5. Apatite and other phosphates

The possible occurrence of liquid–liquid phase separation in calcium phosphate (CaP) mineralization shares many similarities with $CaCO_3$ systems (Fig. 7). Initial reports focused on CaP formation in the presence of polymers, where liquid-like behavior of amorphous precursors—here also termed polymer-induced liquid-precursors (PILP)—was inferred from several key observations. These include the ability of amorphous CaP phases to infiltrate collagen matrices through apparent capillary action[16,31,81–83] (Fig. 7d) and the formation of spherulitic growth patterns in micron-sized CaP spheres.[84] While these phenomena collectively suggest the formation of a liquid-like amorphous phase, quantitative evidence for finite viscosity has remained absent from the literature. Such evidence would be particularly valuable given the current understanding that PILP phases of both $CaCO_3$ and CaP (Fig. 7c) are not molecular liquids, but rather assemblies of nanometer-sized clusters stabilized by polymer interactions[32] – which could easily be confused with solid-state amorphous networks.

In polymer-free systems, early studies reported similar nanocluster assemblies (Fig. 7a), although neither Dey *et al.*[85] nor Habraken *et al.*[86] explicitly invoked liquid–liquid phase

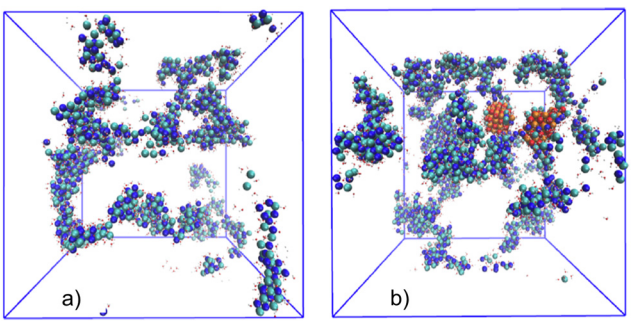

Fig. 6 Snapshots from a molecular dynamics simulation of a NaCl solution in the spinodal domain (18.5 mol kg^{-1}). a) after 10 ns, and b) after 70 ns. Ions with less than 8 neighbors are omitted. Orange particles show crystalline domains. Reprinted with permission from Jiang *et al.*[78] Copyright 2019 American Chemical Society.

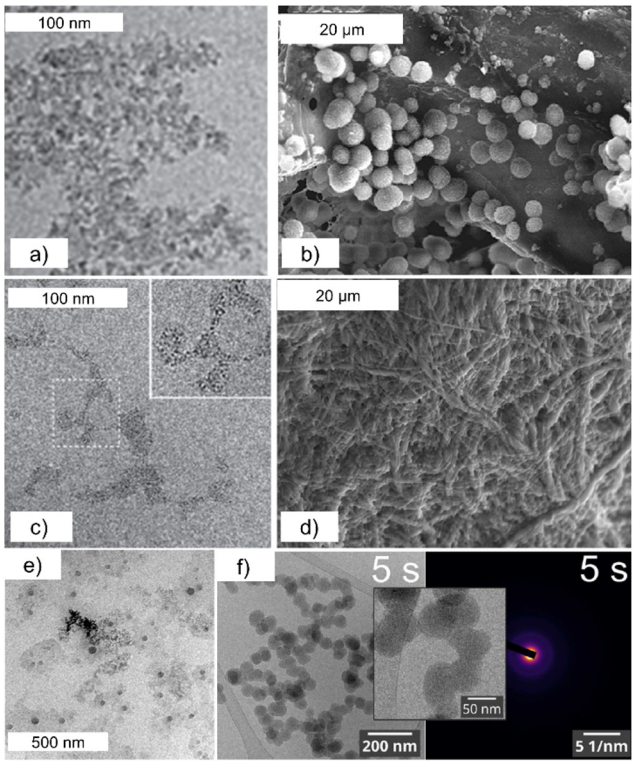

Fig. 7 Experimental investigation of LLPS in phosphate phases. a) Cryo-TEM of a crystallizing calcium phosphate solution after 10 min of reaction. Adapted with permission from Nudelman *et al.*[32] Copyright 2010 Springer Nature. The limited resolution stems from a magnification of the original image, to ensure consistency with the following images. b) SEM of a collagen matrix impregnated for 4 days with a calcium phosphate solution. Adapted with permission from Jee *et al.*[31] Copyright 2010 Elsevier. The calcium phosphate particles are interpreted as an inefficient impregnation in the absence of LLPS. c) Cryo-TEM of a crystallizing calcium phosphate solution in presence of polyaspartate after 10 min of reaction. Adapted with permission from Nudelman *et al.*[32] Copyright 2010 Springer Nature. d) SEM of a collagen matrix impregnated 3 days with a calcium phosphate solution in the presence of polyaspartate. The absence of particles is interpreted as a better wetting of a PILP of calcium phosphate. Adapted with permission from Jee *et al.*[31] Copyright 2010 Elsevier. e) LP TEM of a CaP solution, unspecified reaction time, evidencing a less electron-dense corona around particles. Adapted with permission from Dalmônico *et al.*[35] Copyright 2022 American Chemical Society. f) Cryo-TEM and diffraction of a crystallizing struvite solution after 5 s of reaction, from Karafiludis *et al.*[33] Copyright 2023 American Chemical Society.

separation. Instead, these authors debated whether the observed nanoclusters represented 'pre-nucleation clusters' following the Betts and Posner model,[87] or ion association complexes. Because of their corrugated morphologies, the shapes observed in these systems are not typically reminiscent of liquid phases – unless observed at coarser resolution, as is typically the case in LP TEM. Similarly, collagen matrices impregnated with CaP without polymers show surface deposits of mineral nodules, presented as an evidence for the lack of liquid–liquid phase separation (Fig. 7b). Two recent LP TEM observations finally claimed evidence for LLPS: He *et al.*[34] evidenced a reactant-rich liquid as dark-contrast zones from which the formation of amorphous and crystalline apatite occurs, and Dalmônico *et al.*[35] additionally reported a liquid phase forming mainly onto the observation windows. However, in our opinion, the out-of-equilibrium morphologies and the lack of shape fluctuation are compatible with solid-state nanocluster assemblies (Fig. 7e) – or at least, extremely low capillary velocities. Critically, no dynamic behaviors characteristic of liquids—such as coalescence or relaxation to equilibrium shapes—have been documented, leaving the actual viscosity of these liquid states uncharacterized.

CaP formation with and without additives involves aggregated nanometer-sized structures. At least with polymers, sufficient indirect evidence indicates that separating structures are 'liquid-like'. However, whether such hybrid assemblies can be properly described using liquid–liquid phase separation diagrams typically applied to molecular liquid systems remains undetermined.

Recent advances have extended beyond calcium-based systems to other phosphate-based phases. Karafiludis *et al.*[33] reported the formation of struvite ($MgNH_4PO_4{\cdot}6H_2O$) through a liquid precursor pathway, observing the formation of dense liquid particles in cryo-TEM (Fig. 7f). The liquid character of these precursor phases was demonstrated through the observation of coalescence morphologies. Notably, the SAXS patterns presented in their study appear to rule out the possibility that these liquid phases consist of discrete nanometer-sized clusters, but instead support nanometer-scale concentration fluctuations (*ca.* 1 nm) that preceded the formation of the dense liquid.

2.6. Sulfates

In barium sulfate ($BaSO_4$) syntheses, liquid–liquid phase separation has been proposed based on transmission electron microscopy observations of barite nanoparticles within larger amorphous structures exhibiting liquid-like morphologies, or amorphous liquid-like structures with morphologies reminiscent of coalescing droplets (Fig. 8).[36,37] Energy-dispersive X-ray spectroscopy analysis confirmed these structures to be enriched in barium and sulfur, presumably in a hydrated state. Similar phenomena have been reported in the presence of added polymers, where PILP-like behavior analogous to that observed in

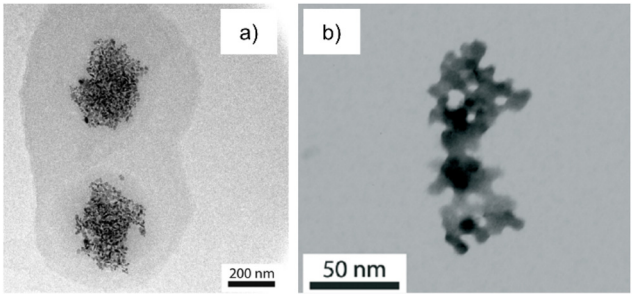

Fig. 8 Experimental investigation of LLPS in barium sulfate. a) TEM of a solution quenched by ethanol addition. Reproduced from Ruiz-Agudo.[36] Copyright 2015 American Chemical Society. b) STEM-HAADF of a solution quenched by ethanol addition. Reproduced from Ruiz-Agudo *et al.*[37] with permission from The Royal Society of Chemistry.

$CaCO_3$ systems was documented. Importantly, the authors suggest that polymers do not induce LLPS in $BaSO_4$ but rather stabilize pre-existing liquid–liquid separation tendencies. However, the observations on $BaSO_4$ were obtained following ethanol quenching and drying procedures for TEM preparation, which may influence the preserved morphologies. Given the preliminary nature of these findings and the potential artifacts associated with the sample preparation methods, the authors appropriately call for further studies to rigorously test the LLPS hypothesis in barium sulfate mineralization.

2.7. Sulfur hydrosols

In 1950, LaMer and Dinegar described the synthesis of sulfur particles in water, establishing foundational concepts for nanoparticle formation through nucleation processes.[38,88] Modern researchers working on nucleation fundamentals will appreciate rediscovering their description of the process as "yielding droplets of supercooled liquid lambda sulfur", with high precursor concentrations producing a characteristic "white milk of sulfur". Importantly, they observed crystallization only at later stages, supporting a long-lived liquid intermediate phase. Contemporary restatements of these observations can be found in Steudel's comprehensive work.[39] The decomposition of sodium hydrogen thiosulfate in dilute hydrochloric acid represents one of several established methods for producing suspensions of sulfur-rich liquid particles (comprising sulfur oligomers and polythionates) at room temperature. These sulfur droplets exist as metastable phases, as the melting point of sulfur is 112 °C, and eventually transform into crystals of α-S_8.

A consensus exists regarding the liquid nature of the transient sulfur particles and their subsequent transition to crystalline phases. However, experimental characterization remains limited: literature reports focus primarily on the bulk suspension viscosity (reaching "honey-like viscosity"[39] at concentrations of 600 g L^{-1}) rather than the intrinsic properties of the liquid forming the individual particles. The liquid character is primarily assessed through thermal behavior

analysis of concentrated sols at sulfur's melting point, where the absence of abrupt viscosity changes is interpreted as evidence that sulfur exists in a liquid state. This interpretation requires careful consideration, as concentrated colloidal suspensions of solid-state nanoparticles (such as SiO_2) can exhibit macroscopically liquid-like behavior.[89]

The mechanism governing the transition from liquid droplets to crystals remains a subject of ongoing debate. LaMer and Dinegar originally postulated what would now be termed classical (direct) nucleation from dissolved monomers, accompanied by secondary nucleation through contact between crystal nuclei and metastable droplets. In contrast, Steudel proposes a multistep nucleation mechanism, reasoning that "the unit cell consists of not less than 16 molecules which have to be oriented in a special manner. This ordering process is hindered first by the impurities present in the dirty cluster and second by the high viscosity liquid sulfur must exhibit at 20 °C".[90] Regarding the formation of the liquid droplets themselves, Lamer has established this system as a paradigm for nucleation, supported by the critical (in the physical sense) nature of the transition: the white milk of sulfur forms abruptly above a given concentration. However, a modern analysis by Whitehead *et al.* has since objected that the large colloids observed by LaMer are far from critical sizes typically expected, and that the quantitative evolution of turbidity deviates from a classical description of nucleation.[88]

In summary, sulfur represents a widely accepted paradigm of liquid-mediated nucleation in mineral systems, with the liquid nature of the intermediate phase being generally acknowledged within the crystallization community. However, despite this widespread acceptance, to our knowledge, no modern *in situ* characterization techniques have been systematically applied to definitively confirm the liquid properties of sulfur droplets or to elucidate the detailed transition mechanisms at the molecular level.

2.8. Oxides

It is admitted that the synthesis of oxides by co-precipitation is prone to forming disordered metastable phases after the hydrolysis and condensation of metal ions, and that achieving better crystallinity often requires thermal annealing.[91] The transient states are almost always reported as solid-state, amorphous particles or fractal aggregates. However, Haberkorn *et al.* reported in 2003 liquid–liquid phase separation in the synthesis of boehmite (AlO(OH)) by acid neutralization of aluminum hydroxide:[40]

$$H_2SO_4 + 2Na[Al(OH)_4] \rightarrow 2AlO(OH) + Na_2SO_4 + 4H_2O$$

Using cryo-TEM 10 ms after mixing, they reported that "a droplet-like structure can be seen frozen in" with sizes between 10 to 300 nm. They inferred the liquid character of the structures from their beaded morphology, supported by the fact that they started degrading and bubbling under the electron beam (Fig. 9a). Beam-resistant particles, attributed to solid-state particles, form within 40 ms of reaction, then convert into the characteristic needle-shaped boehmite crystals.

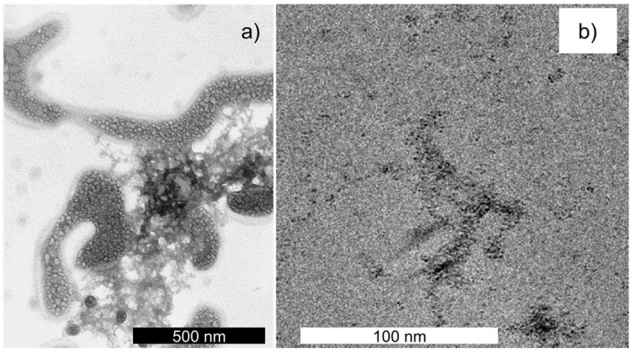

Fig. 9 Experimental investigation of LLPS in oxides a) cryo-TEM prior to boehmite crystallization, freezed *ca.* 10 ms after reaction. Adapted with permission from Haberkorn *et al.*[40] Copyright 2003 Elsevier. Bubbling is induced by the electron beam to demonstrate the difference between the dense liquid precursor and solid-state amorphous particles. b) Cryo-TEM prior to magnetite crystallization, aliquot of a dilute HCl solution titrated with a $FeCl_3$ solution. Adapted with permission from Scheck *et al.*[41] Copyright 2016 American Chemical Society. The granular structure is assigned to pre-nucleation clusters.

Regarding the formation of the liquid structures themselves, Haberkorn *et al.* posit that mixing heterogeneity leads to the formation of reagent droplets at the output of the mixer nozzle. Indeed, both reagents are mixed thought a simple T-junction, and the authors raised concerns about the solution reaching molecular-scaled homogeneity before cryogenic quenching. Back in 2003, the transient liquid structures were therefore not assigned to an underlying thermodynamic phase diagram, but rather to a kinetic hydrodynamic origin – a position overlooked nowadays.

For magnetite formation *via* iron salt hydrolysis, Kashyap *et al.* reported a "liquid-like, disordered pre-nucleation phase" prior to crystallization in the presence of Mms6 protein.[92] While they provided evidence for an amorphous layer forming at vesicle surfaces, the actual liquid character remains unconfirmed. Subsequently, Scheck *et al.* observed aggregated nanometer-sized structures interpreted as pre-nucleation clusters in additive-free syntheses (Fig. 9b).[93] Drawing on controversial calcium carbonate developments, they cautiously proposed that interface formation "may be conceived as passing a liquid–liquid binodal". Building on this hypothesis, Kuhrts *et al.* rationalized organic additive effects on magnetite nanoparticle size by invoking the wetting properties of transient liquid-like ferrihydrite:[94] "approximating the ferrihydrite precursor as a liquid, [Scheck 2016][93] we treat its interaction with magnetite as a wetting process". Although magnetite formation *via* non-crystalline particles is well-established,[95,96] the liquid-state nature of these transient intermediates remains hypothetical and requires direct experimental validation.

2.9. Metal Organic Frameworks

Metal–organic frameworks (MOFs) are porous supramolecular structures of metal cations linked by organic ligands, and zeolitic imidazolate frameworks (ZIFs) are a class of MOFs with zeolite topologies. Of this diverse range of materials, one of the most studied syntheses is of the prototypical ZIF-8, which contains a core comprising a single zinc(II) ion coordinated by imidazolate linkers to form a tetrahedral structure.[97] ZIF-8 is prepared at ambient conditions by mixing zinc salt solutions (zinc acetate or nitrate) with excess imidazole (typically 2-methylimidazole). Syntheses occur in water, alcohol (methanol/ethanol), or water–alcohol mixtures. Alcohol-based syntheses rapidly produce monodisperse ~50 nm crystalline particles (in seconds to minutes).[42,98] Water-based syntheses yield larger particles (100 s of nm) with longer induction times (>1 min), where the nucleation rate and crystal shape are controlled using organic additives like CTAB and proteins.[45,99]

There is no doubt that ZIF-8 formation follows a non-classical pathway *via* amorphous intermediates. Cravillon *et al.* first reported non-crystalline transient phases in ZIF-8 synthesis using time-resolved Small- and Wide Angle X-ray Scattering (SAXS/WAXS), observing the immediate formation of *ca.* 1 nm clusters followed by the growth of larger nanoscale particles that crystallized within 15 s, providing strong evidence for the initial precipitation of an amorphous precursor phase.[42] Subsequent studies by Terban *et al.*[43] and Carraro *et al.*[44] confirmed these results, unequivocally demonstrating a long-lived amorphous (implicitly, solid) phase prior to ZIF-8 crystallization, with increased stability of this transient phase in water compared to methanol.

In this context, Liu *et al.*[45] first suggested a liquid precursor phase in ZIF-8 synthesis based on liquid-cell and cryo-TEM observations of aqueous synthesis (Fig. 10). However, while their cryo-TEM images show "liquid-like" structures, their actual liquid character remains undemonstrated: liquid-cell TEM videos lack temporal and spatial resolution and show no clear structural progression. Additionally, they provided no quantification of density, chemistry, or putative fluid properties, and few subsequent reports corroborate their findings. Jongert *et al.* reported LLPS based on *in situ* electrochemical measurements of particles with positive *z*-potential during the first two minutes of methanolic syntheses,[97] yet these results do not unambiguously confirm a transient liquid phase. Another cryo-TEM study by Ogata *et al.*[100] investigated aqueous ZIF-8 synthesis at varying imidazole : Zn ratios with and without bovine serum albumin, observing various amorphous phases leading to crystals through dissolution–reprecipitation and solid-state transformations, but reported no liquid precursor phase.

Dok *et al.* used *in situ* harmonic light scattering and NMR to follow the nucleation of ZIF-8 crystals in methanol,[101] demonstrating formation of positively charged clusters 'instantaneously' upon mixing. They interpreted these results as PNCs that release protons and condense into amorphous particles before crystallizing. This supports earlier claims of amorphous transient phases; however, more work is required to reconcile competing theories regarding condensed phase formation through PNCs *versus* LLPS. Recent MOF and ZIF-8 nucleation modeling has examined non-classical mechanisms but has not evidenced or considered LLPS, instead focusing on cluster formation, including disordered "glassy clusters", dependent on solvent and kinetic factors.[102,103] Therefore, evidence for non-classical nucleation pathways in ZIF-8 crystallization is strong, but more data are needed to confirm the involvement of liquid–liquid phase separation.

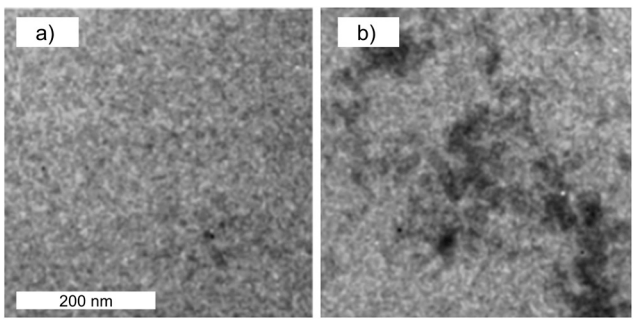

Fig. 10 Experimental investigation of LLPS in ZIF-8. Cryo-TEM of the solution frozen a) 10 s and b) 60 s after mixing, respectively. Adapted with permission from Liu *et al.*[45] Copyright 2021 National Academy of Sciences. The scale bar applies to both images.

3. Conclusion

As 'non-classical nucleation' (*i.e.*, multistep crystallization) pathways have become increasingly recognized as standard mechanisms in crystallization, liquid–liquid phase separation (LLPS) is naturally being discussed in a growing number of mineral systems. However, detecting and characterizing these processes remains remarkably elusive. Detection of non-crystalline transient states in crystallization processes is now increasingly accessible, thanks to techniques that evidence simultaneously the emergence of particles and their amorphous character: cryo-TEM combined with electron diffraction, SAXS (with $q < 0.5$ A^{-1}) combined with WAXS ($q > 1$ A^{-1}), and LP TEM – although the combination with electron diffraction and the proper definition of reaction time and supersaturation are more demanding with this technique. This has increasingly popularized the idea of LLPS and leads to more mature fundamental questions in the field (Fig. 1).

First, characterizing not only the presence but the emergence itself of transient structures (liquid or not) remains a huge experimental challenge (Fig. 1a), motivated by questions regarding LLPS mechanisms *via* ion pairs, PNCs, nucleation, spinodal decomposition, *etc.* Although nanometer-scale resolution is technically accessible today, time resolution remains limited. Reaction times in LP-TEM are ill-defined because of overly simple mixers in state-of-the-art liquid sample holders, creating a fundamental bottleneck due to supersaturation drops when the parent solution starts

evolving. Although millisecond resolution has been reached in SAXS, some reports show this is still insufficient.[24,25,74,96,104] A first perspective in the field is to push the boundaries of time resolution, presumably with advanced microfluidic tools.[105]

Second, definitively establishing the 'liquid' character of observed precursor phases, in terms of physical dynamics (*e.g.*, viscosity), remains a challenge (Fig. 1b). While state-of-the-art cryo-TEM and SAXS/WAXS analyses ensure detection down to a few milliseconds after reaction, these static techniques are blind to visco-elastic properties and therefore unsuitable for distinguishing between liquid and solid amorphous structures. Past intuitions and postulates based on macroscopic and indirect evidence have proven correct in several emblematic cases, suggesting that simpler analytical approaches should not be overlooked in the pursuit of more sophisticated characterization methods. These simple approaches should nowadays be systematically validated with AFM and LP TEM, which enable testing directly true liquid behavior, including droplet coalescence. However, caution should be taken because these techniques are only able to access viscosities starting around five orders of magnitude higher than water. Thus, the typical 'liquid-like' displacements accessible by electron microscopy (nanometer scale) over experimental time resolutions (seconds, up to several days in impregnation experiments) correspond to capillary velocities similar to those of tar (nm s^{-1}), and would be classified as solid or at least "gel-like" at typical laboratory scales. The "liquid-like" behavior even observed directly may actually reflect extremely viscous flow over nanometer distances and minute timescales rather than true liquid dynamics. This interpretation challenge is compounded by the already discussed issues of representativeness in LP TEM observations, including electron beam effects and confinement artifacts. A second perspective in the field is to use systematically methods (AFM, LP-TEM) that distinguish solid-state and true liquid amorphous phases, with the even more challenging prospect of systematically measuring viscosity. Development of alternative techniques less prone to electron beam damage or interference from SiN membrane surfaces is strongly needed.

Further, while the term "liquid" usually refers to molecular or ionic liquids, many have reported LLPS involving aggregated primary nanoparticles (such as in PILP systems and cluster clouds, and in some of the debated PNC pathways). In these colloidal assemblies, the bulk phase may exhibit flow behavior, while individual primary particles might remain in solid-state configurations. This distinction between macroscopic flow properties and microscopic structural states represents a critical aspect of accurate phase characterization. A third perspective in the field is therefore to systematically assess internal structure combined with local dynamics (Fig. 1c), for instance coupling SAXS/WAXS and NMR.

Finally, validating an appropriate theoretical framework represents the last paramount challenge (Fig. 1d). The complexity of this understanding is exacerbated by inconsistent reporting practices, which raises questions about whether LLPS is genuinely absent in unreported cases or simply falls beyond the scope of individual studies. More systematic exploration across different mineral systems is needed as a prerequisite to developing a better phenomenological understanding of LLPS occurrence and, ultimately, comprehensive theoretical frameworks. The dominant consensus describes LLPS through thermodynamic concepts (phase diagrams, equilibrium constants), despite the parent solution being extremely far from equilibrium. In electrolyte systems, this thermodynamic approach aligns with theoretical predictions, particularly for primitive model systems where LLPS is predicted in $+z/-z$ electrolytes with $z > 3.8$ in water using Gibbs ensemble methods.[106] However, alternative mechanisms merit consideration. In the field of thermodynamic models, Stawski *et al.* summarized how the emergence of (solid-state) amorphous transient structures can be rationalized, relying on a balance between either the solubility or interfacial tension of the amorphous phases and the crystal,[107] which are applicable to liquid structures. However, some evidence suggests that kinetic rather than purely thermodynamic factors may govern LLPS processes. Reinvestigation of alternative pathways similar to mixing heterogeneity, irreversible condensation or out-of-equilibrium fluctuations could prove fruitful. Since these systems operate far from equilibrium conditions, the traditional Gibbs phase rule may not apply, potentially allowing for multiple competing pathways and more complex behavior than classical thermodynamic treatments would predict. A final perspective in the field is therefore to integrate experimental and theoretical approaches that can capture both out-of-equilibrium thermodynamics and kinetic factors governing LLPS.

Conflicts of interest

There are no conflicts of interest to declare.

Data availability

No primary research results, software or code have been included and no new data were generated or analysed as part of this review.

Acknowledgements

The authors acknowledge Fabienne Testard, Frédéric Gobeaux, Thomas Philippe, Sébastien Teychené and Isaac Rodríguez Ruiz for stimulating discussions. We acknowledge financial support of the French National Research Agency (ANR-21-CE06-0032).

References

1 P. G. Vekilov, in *ACS Symposium Series*, ed. X. Zhang, American Chemical Society, Washington, DC, 2020, vol. 1358, pp. 19–46.

2 D. Gebauer and H. Cölfen, *Nano Today*, 2011, **6**, 564–584.
3 J. J. De Yoreo, P. U. P. A. Gilbert, N. A. J. M. Sommerdijk, R. L. Penn, S. Whitelam, D. Joester, H. Zhang, J. D. Rimer, A. Navrotsky, J. F. Banfield, A. F. Wallace, F. M. Michel, F. C. Meldrum, H. Cölfen and P. M. Dove, *Science*, 2015, **349**, aaa6760.
4 S. Alberti, A. Gladfelter and T. Mittag, *Cell*, 2019, **176**, 419–434.
5 S. Xu, H. Zhang, B. Qiao and Y. Wang, *Cryst. Growth Des.*, 2021, **21**, 7306–7325.
6 L. A. Gower and D. A. Tirrell, *J. Cryst. Growth*, 1998, **191**, 153–160.
7 S. E. Wolf, J. Leiterer, M. Kappl, F. Emmerling and W. Tremel, *J. Am. Chem. Soc.*, 2008, **130**, 12342–12347.
8 S. E. Wolf, J. Leiterer, V. Pipich, R. Barrea, F. Emmerling and W. Tremel, *J. Am. Chem. Soc.*, 2011, **133**, 12642–12649.
9 J. Rieger, T. Frechen, G. Cox, W. Heckmann, C. Schmidt and J. Thieme, *Faraday Discuss.*, 2007, **136**, 265–277.
10 P. J. M. Smeets, A. R. Finney, W. J. E. M. Habraken, F. Nudelman, H. Friedrich, J. Laven, J. J. De Yoreo, P. M. Rodger and N. A. J. M. Sommerdijk, *Proc. Natl. Acad. Sci. U. S. A.*, 2017, **114**, E7882–E7890.
11 M. A. Bewernitz, D. Gebauer, J. Long, H. Cölfen and L. B. Gower, *Faraday Discuss.*, 2012, **159**, 291–312.
12 A. F. Wallace, L. O. Hedges, A. Fernandez-Martinez, P. Raiteri, J. D. Gale, G. A. Waychunas, S. Whitelam, J. F. Banfield and J. J. D. Yoreo, *Science*, 2013, **341**, 885–889.
13 Z. Zou, W. J. E. M. Habraken, L. Bertinetti, Y. Politi, A. Gal, S. Weiner, L. Addadi and P. Fratzl, *Adv. Mater. Interfaces*, 2017, **4**, 1600076.
14 V. Ramnarain, T. Georges, N. Ortiz Peña, D. Ihiawakrim, M. Longuinho, H. Bulou, C. Gervais, C. Sanchez, T. Azaïs and O. Ersen, *J. Am. Chem. Soc.*, 2022, **144**, 15236–15251.
15 L. B. Gower and D. J. Odom, *J. Cryst. Growth*, 2000, **210**, 719–734.
16 M. J. Olszta, E. P. Douglas and L. B. Gower, *Calcif. Tissue Int.*, 2003, **72**, 583–591.
17 Y.-Y. Kim, E. P. Douglas and L. B. Gower, *Langmuir*, 2007, **23**, 4862–4870.
18 Y.-Y. Kim, N. B. J. Hetherington, E. H. Noel, R. Kröger, J. M. Charnock, H. K. Christenson and F. C. Meldrum, *Angew. Chem., Int. Ed.*, 2011, **50**, 12572–12577.
19 S. L. P. Wolf, L. Caballero, F. Melo and H. Cölfen, *Langmuir*, 2017, **33**, 158–163.
20 M. Farhadi-Khouzani, C. Schütz, G. M. Durak, J. Fornell, J. Sort, G. Salazar-Alvarez, L. Bergström and D. Gebauer, *J. Mater. Chem. A*, 2017, **5**, 16128–16133.
21 Y. Xu, K. C. H. Tijssen, P. H. H. Bomans, A. Akiva, H. Friedrich, A. P. M. Kentgens and N. A. J. M. Sommerdijk, *Nat. Commun.*, 2018, **9**, 2582.
22 B. Jin, Y. Chen, H. Pyles, M. D. Baer, B. A. Legg, Z. Wang, N. M. Washton, K. T. Mueller, D. Baker, G. K. Schenter, C. J. Mundy and J. J. De Yoreo, *Nat. Mater.*, 2024, 1–8.
23 I. Rodríguez-Ruiz, S. Charton, D. Radajewski, T. Bizien and S. Teychené, *CrystEngComm*, 2018, **20**, 3302.
24 M. Durelle, S. Charton, F. Gobeaux, C. Chevallard, L. Belloni, F. Testard, S. Trépout and D. Carriere, *J. Phys. Chem. Lett.*, 2022, **13**, 8502–8508.
25 J. Raimbault, C. Chevallard, D. Ihiawakrim, V. Ramnarain, O. Ersen, F. Gobeaux and D. Carriere, *Nano Lett.*, 2025, **26**, 2275–2282.
26 Y. Mikhlin, M. Likhatski, A. Karacharov, V. Zaikovski and A. Krylov, *Phys. Chem. Chem. Phys.*, 2009, **11**, 5445–5454.
27 Y. Mikhlin, A. Karacharov, M. Likhatski, T. Podlipskaya, Y. Zubavichus, A. Veligzhanin and V. Zaikovski, *J. Colloid Interface Sci.*, 2011, **362**, 330–336.
28 N. D. Loh, S. Sen, M. Bosman, S. F. Tan, J. Zhong, C. A. Nijhuis, P. Král, P. Matsudaira and U. Mirsaidov, *Nat. Chem.*, 2017, **9**, 77–82.
29 B. Jin, Y. Wang, Z. Liu, A. France-Lanord, J. C. Grossman, C. Jin and R. Tang, *Adv. Mater.*, 2019, **31**, 1808225.
30 G. Li, N. He, J. Deng, J. Liu, Y. Sun, M. Qu, Y. Jiang, T. Zhao, S.-Y. Zhou, H. Zeng, Q. Zheng, H.-G. Liao and S.-G. Sun, *Cryst. Growth Des.*, 2021, **21**, 6025–6030.
31 S.-S. Jee, T. T. Thula and L. B. Gower, *Acta Biomater.*, 2010, **6**, 3676–3686.
32 F. Nudelman, K. Pieterse, A. George, P. H. H. Bomans, H. Friedrich, L. J. Brylka, P. A. J. Hilbers, G. de With and N. A. J. M. Sommerdijk, *Nat. Mater.*, 2010, **9**, 1004–1009.
33 S. Karafiludis, E. Scoppola, S. E. Wolf, Z. Kochovski, D. Matzdorff, A. E. S. Van Driessche, J. Hövelmann, F. Emmerling and T. M. Stawski, *J. Chem. Phys.*, 2023, **159**, 134503.
34 K. He, M. Sawczyk, C. Liu, Y. Yuan, B. Song, R. Deivanayagam, A. Nie, X. Hu, V. P. Dravid, J. Lu, C. Sukotjo, Y. Lu, P. Král, T. Shokuhfar and R. Shahbazian-Yassar, *Sci. Adv.*, 2020, **6**, eaaz7524.
35 G. M. L. Dalmônico, D. Ihiawakrim, N. Ortiz, A. G. Barreto Junior, C. F. Curitiba Marcellos, M. Farina, O. Ersen and A. L. Rossi, *Cryst. Growth Des.*, 2022, **22**, 4828–4837.
36 C. Ruiz-Agudo, E. Ruiz-Agudo, C. V. Putnis and A. Putnis, *Cryst. Growth Des.*, 2015, **15**, 3724–3733.
37 C. Ruiz-Agudo, D. McDonogh, J. T. Avaro, D. J. Schupp and D. Gebauer, *CrystEngComm*, 2020, **22**, 1310–1313.
38 V. K. LaMer and R. H. Dinegar, *J. Am. Chem. Soc.*, 1950, **72**, 4847–4854.
39 R. Steudel, in *Elemental Sulfur and Sulfur-Rich Compounds I*, ed. R. Steudel, Springer, Berlin, Heidelberg, 2003, pp. 153–166.
40 H. Haberkorn, D. Franke, T. Frechen, W. Goesele and J. Rieger, *J. Colloid Interface Sci.*, 2003, **259**, 112–126.
41 J. Scheck, B. Wu, M. Drechsler, R. Rosenberg, A. E. S. Van Driessche, T. M. Stawski and D. Gebauer, *J. Phys. Chem. Lett.*, 2016, **7**, 3123–3130.
42 J. Cravillon, C. A. Schröder, R. Nayuk, J. Gummel, K. Huber and M. Wiebcke, *Angew. Chem., Int. Ed.*, 2011, **50**, 8067–8071.
43 M. W. Terban, D. Banerjee, S. Ghose, B. Medasani, A. Shukla, B. A. Legg, Y. Zhou, Z. Zhu, M. L. Sushko, J. J. D. Yoreo, J. Liu, P. K. Thallapally and S. J. L. Billinge, *Nanoscale*, 2018, **10**, 4291–4300.

44 F. Carraro, J. D. Williams, M. Linares-Moreau, C. Parise, W. Liang, H. Amenitsch, C. Doonan, C. O. Kappe and P. Falcaro, *Angew. Chem., Int. Ed.*, 2020, **59**, 8123–8127.
45 X. Liu, S. W. Chee, S. Raj, M. Sawczyk, P. Král and U. Mirsaidov, *Proc. Natl. Acad. Sci. U. S. A.*, 2021, **118**, e2008880118.
46 M. Faatz, F. Gröhn and G. Wegner, *Adv. Mater.*, 2004, **16**, 996–1000.
47 K. Henzler, E. O. Fetisov, M. Galib, M. D. Baer, B. A. Legg, C. Borca, J. M. Xto, S. Pin, J. L. Fulton, G. K. Schenter, N. Govind, J. I. Siepmann, C. J. Mundy, T. Huthwelker and J. J. De Yoreo, *Sci. Adv.*, 2018, **4**, eaao6283.
48 E. M. Pouget, P. H. H. Bomans, J. A. C. M. Goos, P. M. Frederik, G. de With and N. A. J. M. Sommerdijk, *Science*, 2009, **323**, 1455–1458.
49 V. Pipich, M. Balz, S. E. Wolf, W. Tremel and D. Schwahn, *J. Am. Chem. Soc.*, 2008, **130**, 6879–6892.
50 L. Dai, E. P. Douglas and L. B. Gower, *J. Non-Cryst. Solids*, 2008, **354**, 1845–1854.
51 B. Cantaert, A. Verch, Y.-Y. Kim, H. Ludwig, V. N. Paunov, R. Kröger and F. C. Meldrum, *Chem. Mater.*, 2013, **25**, 4994–5003.
52 A. S. Schenk, H. Zope, Y.-Y. Kim, A. Kros, N. A. J. M. Sommerdijk and F. C. Meldrum, *Faraday Discuss.*, 2013, **159**, 327–344.
53 Z. Zhang, D. Gao, H. Zhao, C. Xie, G. Guan, D. Wang and S.-H. Yu, *J. Phys. Chem. B*, 2006, **110**, 8613–8618.
54 N. A. J. M. Sommerdijk, E. N. M. van Leeuwen, M. R. J. Vos and J. A. Jansen, *CrystEngComm*, 2007, **9**, 1209–1214.
55 J. K. Berg, T. Jordan, Y. Binder, H. G. Börner and D. Gebauer, *J. Am. Chem. Soc.*, 2013, **135**, 12512–12515.
56 D. Gebauer, A. Völkel and H. Cölfen, *Science*, 2008, **322**, 1819–1822.
57 M. Kellermeier, P. Raiteri, J. K. Berg, A. Kempter, J. D. Gale and D. Gebauer, *ChemPhysChem*, 2016, **17**, 3535–3541.
58 F. Sebastiani, S. L. P. Wolf, B. Born, T. Q. Luong, H. Cölfen, D. Gebauer and M. Havenith, *Angew. Chem., Int. Ed.*, 2017, **56**, 490–495.
59 J. T. Avaro, S. L. P. Wolf, K. Hauser and D. Gebauer, *Angew. Chem., Int. Ed.*, 2020, **59**, 6155–6159.
60 J. Avaro, E. M. Moon, K. G. Schulz and A. L. Rose, *J. Phys. Chem. Lett.*, 2023, **14**, 4517–4523.
61 H. Mohanram, T. Georges, K. Pervushin, T. Azaïs and A. Miserez, *Chem. Mater.*, 2021, **33**, 9715–9724.
62 Z. Zou, L. Bertinetti, Y. Politi, P. Fratzl and W. J. E. M. Habraken, *Small*, 2017, **13**, 1603100.
63 A. R. Finney, R. Innocenti Malini, C. L. Freeman and J. H. Harding, *Cryst. Growth Des.*, 2020, **20**, 3077–3092.
64 P. Raiteri, A. Schuitemaker and J. D. Gale, *J. Phys. Chem. B*, 2020, **124**, 3568–3582.
65 R. Demichelis, P. Raiteri, J. D. Gale, D. Quigley and D. Gebauer, *Nat. Commun.*, 2011, **2**, 590.
66 S. E. Wolf, L. Müller, R. Barrea, C. J. Kampf, J. Leiterer, U. Panne, T. Hoffmann, F. Emmerling and W. Tremel, *Nanoscale*, 2011, **3**, 1158.
67 D. Gebauer, P. Raiteri, J. D. Gale and H. Cölfen, *Am. J. Sci.*, 2018, **318**, 969–988.
68 L. Gower and J. Elias, *J. Struct. Biol.: X*, 2022, **6**, 100059.
69 M. A. Bewernitz, *Faraday Discuss.*, 2012, **159**, 387–420.
70 L. B. Gower, *Chem. Rev.*, 2008, **108**, 4551–4627.
71 S. J. Homeijer, R. A. Barrett and L. B. Gower, *Cryst. Growth Des.*, 2010, **10**, 1040–1052.
72 M. Hajir, R. Graf and W. Tremel, *Chem. Commun.*, 2014, **50**, 6534–6536.
73 E. Ruiz-Agudo, A. Burgos-Cara, C. Ruiz-Agudo, A. Ibañez-Velasco, H. Cölfen and C. Rodriguez-Navarro, *Nat. Commun.*, 2017, **8**, 768.
74 M. Durelle, F. Gobeaux, T. K. Truong, S. Charton and D. Carriere, *Cryst. Growth Des.*, 2023, **23**, 5631–5640.
75 T. Yao, Z. Sun, Y. Li, Z. Pan, H. Wei, Y. Xie, M. Nomura, Y. Niwa, W. Yan, Z. Wu, Y. Jiang, Q. Liu and S. Wei, *J. Am. Chem. Soc.*, 2010, **132**, 7696–7701.
76 J. Yang, J. Koo, S. Kim, S. Jeon, B. K. Choi, S. Kwon, J. Kim, B. H. Kim, W. C. Lee, W. B. Lee, H. Lee, T. Hyeon, P. Ercius and J. Park, *J. Am. Chem. Soc.*, 2019, **141**, 763–768.
77 R. K. Ramamoorthy, E. Yildirim, E. Barba, P. Roblin, J. A. Vargas, L.-M. Lacroix, I. Rodriguez-Ruiz, P. Decorse, V. Petkov, S. Teychené and G. Viau, *Nanoscale*, 2020, **12**, 16173–16188.
78 H. Jiang, P. G. Debenedetti and A. Z. Panagiotopoulos, *J. Chem. Phys.*, 2019, **150**, 124502.
79 A. R. Finney and M. Salvalaglio, *Faraday Discuss.*, 2022, **235**, 56–80.
80 P. S. Bulutoglu, S. Wang, M. Boukerche, N. K. Nere, D. S. Corti and D. Ramkrishna, *PNAS Nexus*, 2022, **1**, pgac033.
81 S. S. Jee, R. K. Kasinath, E. DiMasi, Y.-Y. Kim and L. Gower, *CrystEngComm*, 2011, **13**, 2077–2083.
82 S. S. Jee, L. Culver, Y. Li, E. P. Douglas and L. B. Gower, *J. Cryst. Growth*, 2010, **312**, 1249–1256.
83 T. T. Thula, D. E. Rodriguez, M. H. Lee, L. Pendi, J. Podschun and L. B. Gower, *Acta Biomater.*, 2011, **7**, 3158–3169.
84 F. F. Amos, L. Dai, R. Kumar, S. R. Khan and L. B. Gower, *Urol. Res.*, 2009, **37**, 11–17.
85 A. Dey, P. H. H. Bomans, F. A. Müller, J. Will, P. M. Frederik, G. de With and N. A. J. M. Sommerdijk, *Nat. Mater.*, 2010, **9**, 1010–1014.
86 W. J. E. M. Habraken, J. Tao, L. J. Brylka, H. Friedrich, L. Bertinetti, A. S. Schenk, A. Verch, V. Dmitrovic, P. H. H. Bomans, P. M. Frederik, J. Laven, P. van der Schoot, B. Aichmayer, G. de With, J. J. DeYoreo and N. A. J. M. Sommerdijk, *Nat. Commun.*, 2013, **4**, 1507.
87 F. Betts and A. S. Posner, *Mater. Res. Bull.*, 1974, **9**, 353–360.
88 C. B. Whitehead, S. Özkar and R. G. Finke, *Chem. Mater.*, 2019, **31**, 7116–7132.
89 A. B. Bourlinos, E. P. Giannelis, Q. Zhang, L. A. Archer, G. Floudas and G. Fytas, *Eur. Phys. J. E: Soft Matter Biol. Phys.*, 2006, **20**, 109–117.
90 R. Steudel, *Ind. Eng. Chem. Res.*, 1996, **35**, 1417–1423.
91 C. F. Baes and R. E. Mesmer, *The Hydrolysis of Cations*, Wiley, 1976.

92 S. Kashyap, T. J. Woehl, X. Liu, S. K. Mallapragada and T. Prozorov, *ACS Nano*, 2014, **8**, 9097–9106.
93 J. Scheck, B. Wu, M. Drechsler, R. Rosenberg, A. E. S. Van Driessche, T. M. Stawski and D. Gebauer, *J. Phys. Chem. Lett.*, 2016, **7**, 3123–3130.
94 L. Kuhrts, S. Prévost, D. M. Chevrier, P. Pekker, O. Spaeker, M. S. Egglseder, J. Baumgartner, M. Pósfai and D. Faivre, *J. Am. Chem. Soc.*, 2021, **143**, 10963–10969.
95 J. Baumgartner, A. Dey, P. H. H. Bomans, C. Le Coadou, P. Fratzl, N. A. J. M. Sommerdijk and D. Faivre, *Nat. Mater.*, 2013, **12**, 310–314.
96 J. Baumgartner, R. K. Ramamoorthy, A. P. Freitas, M.-A. Neouze, M. Bennet, D. Faivre and D. Carriere, *Nano Lett.*, 2020, **20**, 5001–5007.
97 T. K. Jongert, I. A. Slowinski, B. Dao, V. H. Cortez, T. Gredig, N. D. Plascencia and F. Tian, *Langmuir*, 2024, **40**, 6138–6148.
98 J. Cravillon, S. Münzer, S.-J. Lohmeier, A. Feldhoff, K. Huber and M. Wiebcke, *Chem. Mater.*, 2009, **21**, 1410–1412.
99 N. K. Maddigan, A. Tarzia, D. M. Huang, C. J. Sumby, S. G. Bell, P. Falcaro and C. J. Doonan, *Chem. Sci.*, 2018, **9**, 4217–4223.
100 A. F. Ogata, A. M. Rakowski, B. P. Carpenter, D. A. Fishman, J. G. Merham, P. J. Hurst and J. P. Patterson, *J. Am. Chem. Soc.*, 2020, **142**, 1433–1442.
101 A. R. Dok, S. Radhakrishnan, F. de Jong, E. Becquevort, O. Deschaume, C. V. Chandran, Y. de Coene, C. Bartic, M. Van der Auweraer, W. Thielemans, C. Kirschhock, M. A. van der Veen, T. Verbiest, E. Breynaert and S. Van Cleuvenbergen, *J. Am. Chem. Soc.*, 2025, **147**, 8455–8466.
102 S. R. G. Balestra, B. Martínez-Haya, N. Cruz-Hernández, D. W. Lewis, S. M. Woodley, R. Semino, G. Maurin, A. R. Ruiz-Salvador and S. Hamad, *Nanoscale*, 2023, **15**, 3504–3519.
103 L. Kollias, R. Rousseau, V.-A. Glezakou and M. Salvalaglio, *J. Am. Chem. Soc.*, 2022, **144**, 11099–11109.
104 A. P. Freitas, R. K. Ramamoorthy, M. Durelle, E. Larquet, I. Maurin, F. Testard, C. Chevallard, T. Gacoin and D. Carriere, *Nano Lett.*, 2021, **22**, 29–35.
105 M. A. Levenstein, C. Chevallard, F. Malloggi, F. Testard and O. Taché, *Lab Chip*, 2025, **25**, 1169–1227.
106 G. Orkoulas and A. Z. Panagiotopoulos, *J. Chem. Phys.*, 1994, **101**, 1452–1459.
107 T. M. Stawski, M. Salvalaglio, A. F. Wallace and J. J. De Yoreo, *Elements*, 2025, **21**, 25–32.

